Supporting Information

Morphology and Optoelectronic Variations Underlying the Nature of the Electron Transport Layer in Perovskite Solar Cells

Wendy J. Nimens,[†] *Jonathan Ogle,*[†] *Anna Caruso,*[‡] *Mackenzie Jonely,*[†] *Charles Simon,*[†] *Detlef Smilgies,*[#] *Rodrigo Noriega,*[†] *Michael Scarpulla,*[‡] *and Luisa Whittaker-Brooks*[†,]*

[†]Department of Chemistry, University of Utah, 315 South 1400 East, Rm 2020, Salt Lake City, Utah, 84112, USA

[‡]Department of Materials Science and Engineering, University of Utah, 315 South 1400 East, Salt Lake City, UT, 84112, USA

[#] Cornell High Energy Synchrotron Source, Cornell University, Ithaca, NY 14853, USA

*Email: **luisa.whittaker@utah.edu**

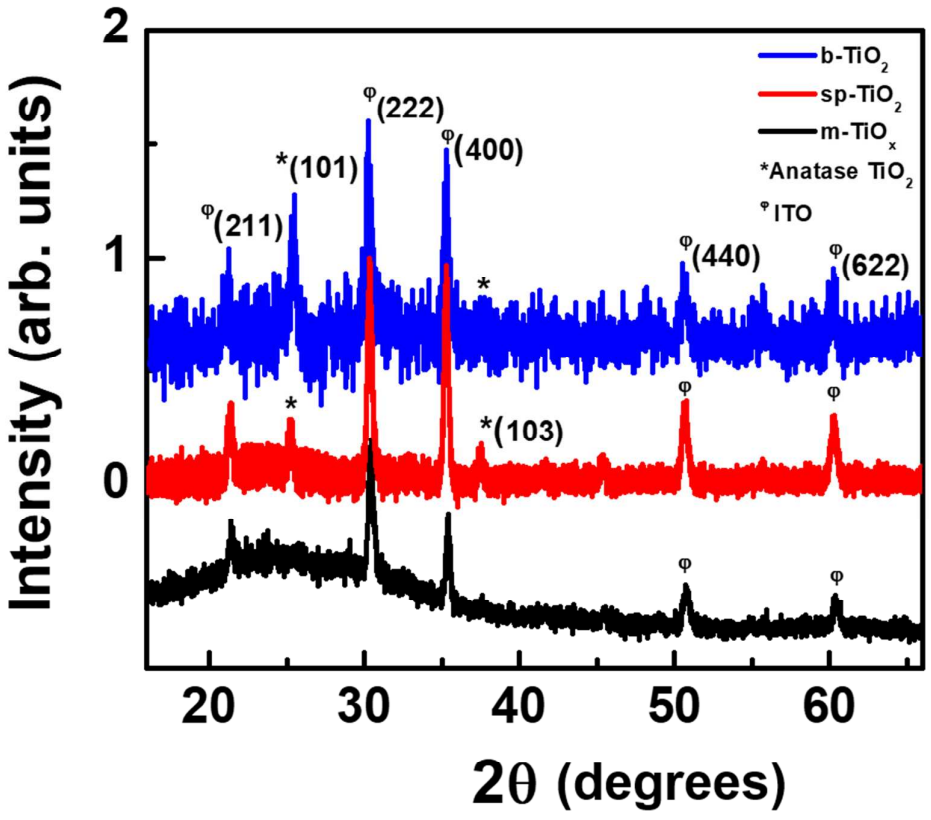

Figure S1. XRD spectra for b-TiO_2, m-TiO_x, and sp-TiO_2 ETLs.

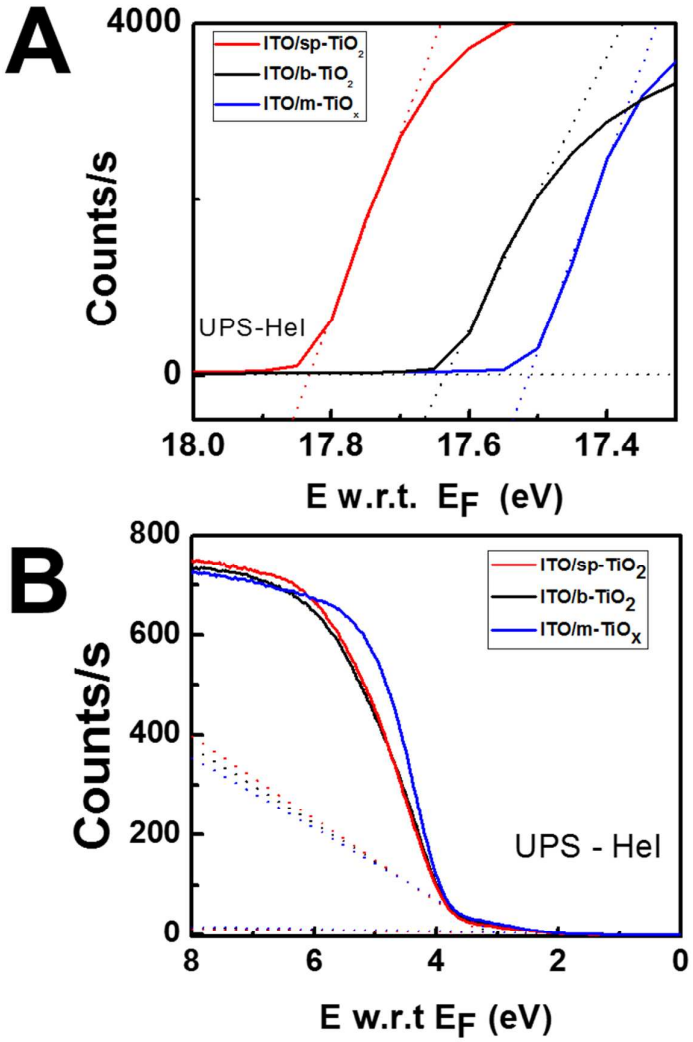

Figure S2. UPS spectra for dense b-TiO_2, m-TiO_x, and sp-TiO_2 ETLs on ITO. **A)** Secondary electron cutoff for work function determination. **B)** Magnification of the UPS spectra close to the Fermi level for the determination of the VBM onset.

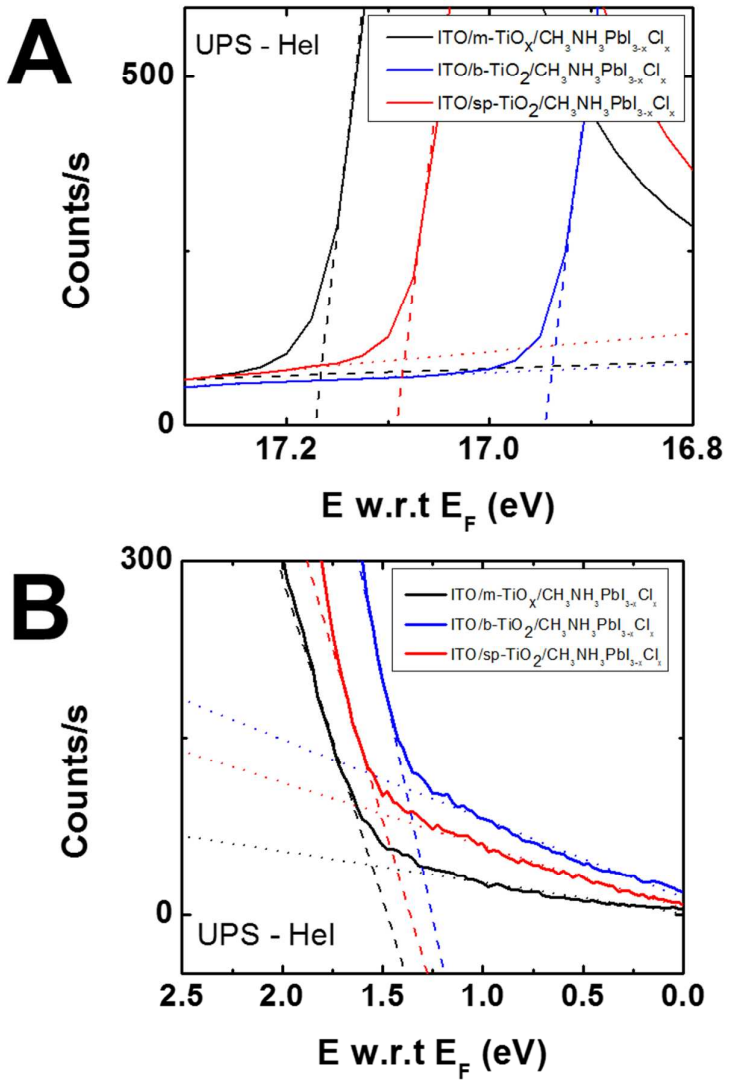

Figure S3. UPS spectra for a 500nm-thick $CH_3NH_3PbI_3$ layer atop the b-TiO_2, m-TiO_x, and sp-TiO_2 ETLs, respectively. **A)** Secondary electron cutoff for work function determination. **B)** Magnification of the UPS spectra close to the Fermi level for the determination of the VBM onset.

Table S1. Device performance of $CH_3NH_3PbI_{3-x}Cl_x$ solar cells atop b-TiO_2, m-TiO_x, and sp-TiO_2.

ETLs (30nm)[a]	**Jsc (mA/cm^2)**	**Voc (V)**	**FF (%)**	**PCE (%)**
b-TiO_2	18.9 ± 1.5	0.77 ± 0.03	41 ± 2	6.0 ± 0.3
m-TiO_x	19.7 ± 1.3	0.76 ± 0.02	49 ± 3	7.3 ± 0.4
sp-TiO_2	23.1 ± 0.8	0.88 ± 0.01	64 ± 1	13.2 ± 0.3

[a]device performance based on 12 devices tested in each batch; $CH_3NH_3PbI_{3-x}Cl_x$ layer was spin-coated at 3000 rpm for 37 s; devices were thermally annealed at 100 ^oC for 120 mins.

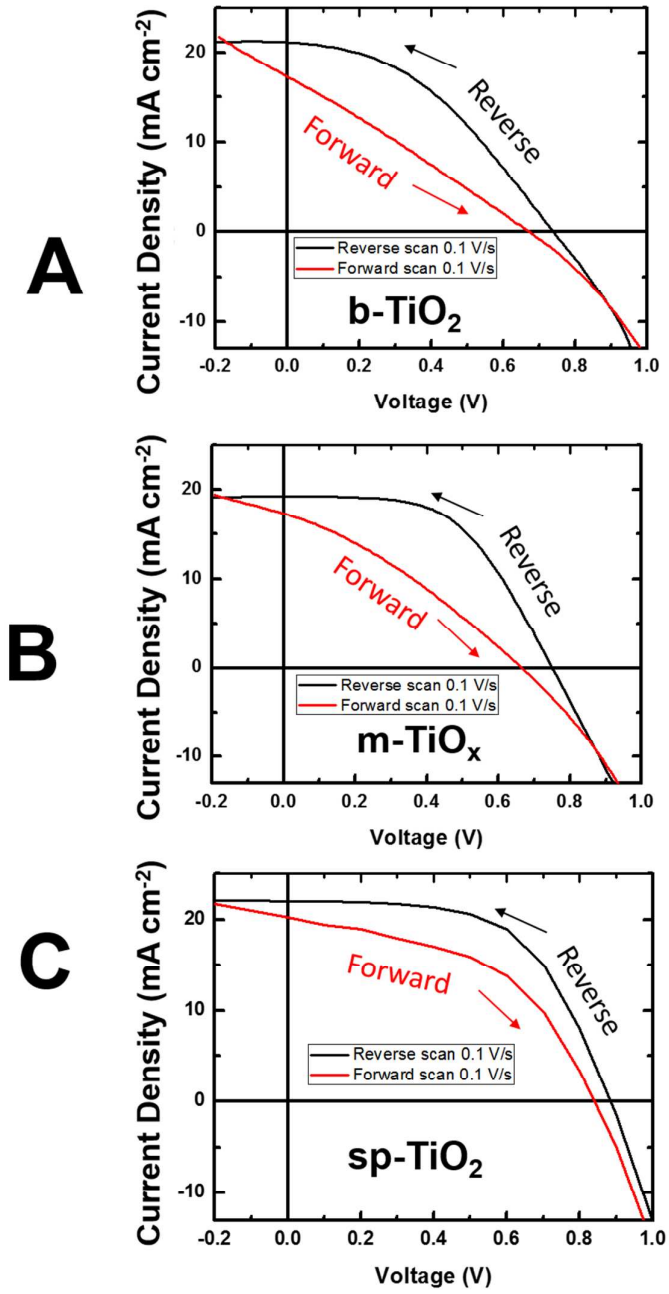

Figure S4. Forward and reverse J-V curves for $CH_3NH_3PbI_{3-x}Cl_x$ deposited atop A) b-TiO_2, B) m-TiO_x, and C) sp-TiO_2 ETLs.

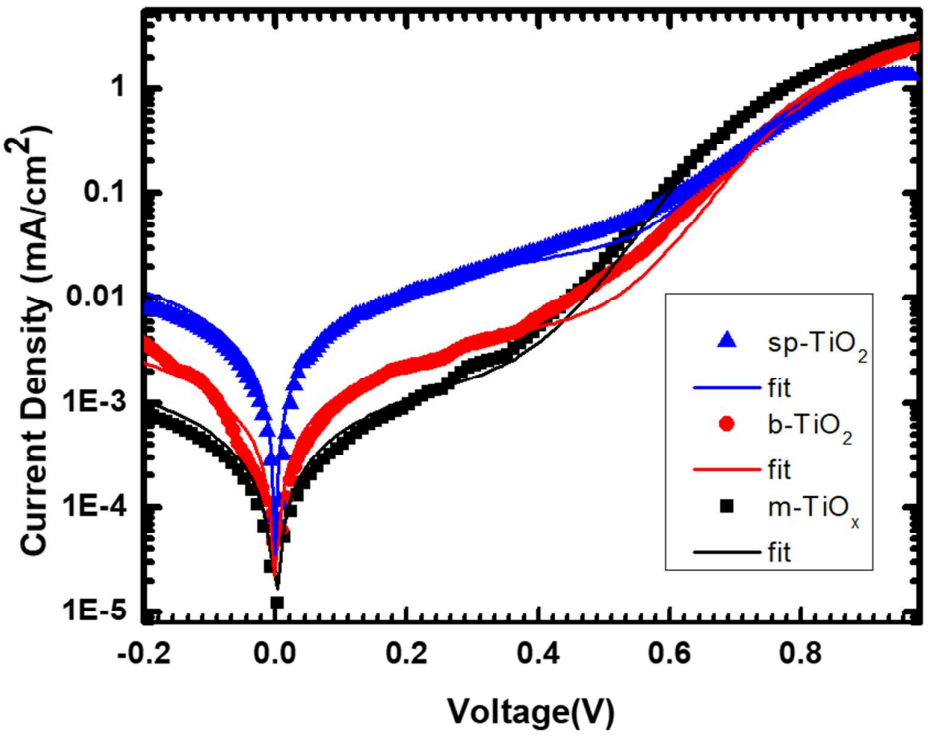

Figure S5. Dark and fit curves for $CH_3NH_3PbI_{3-x}Cl_x$ solar cells deposited atop b-TiO_2, m-TiO_x, and sp-TiO_2 ETLs.

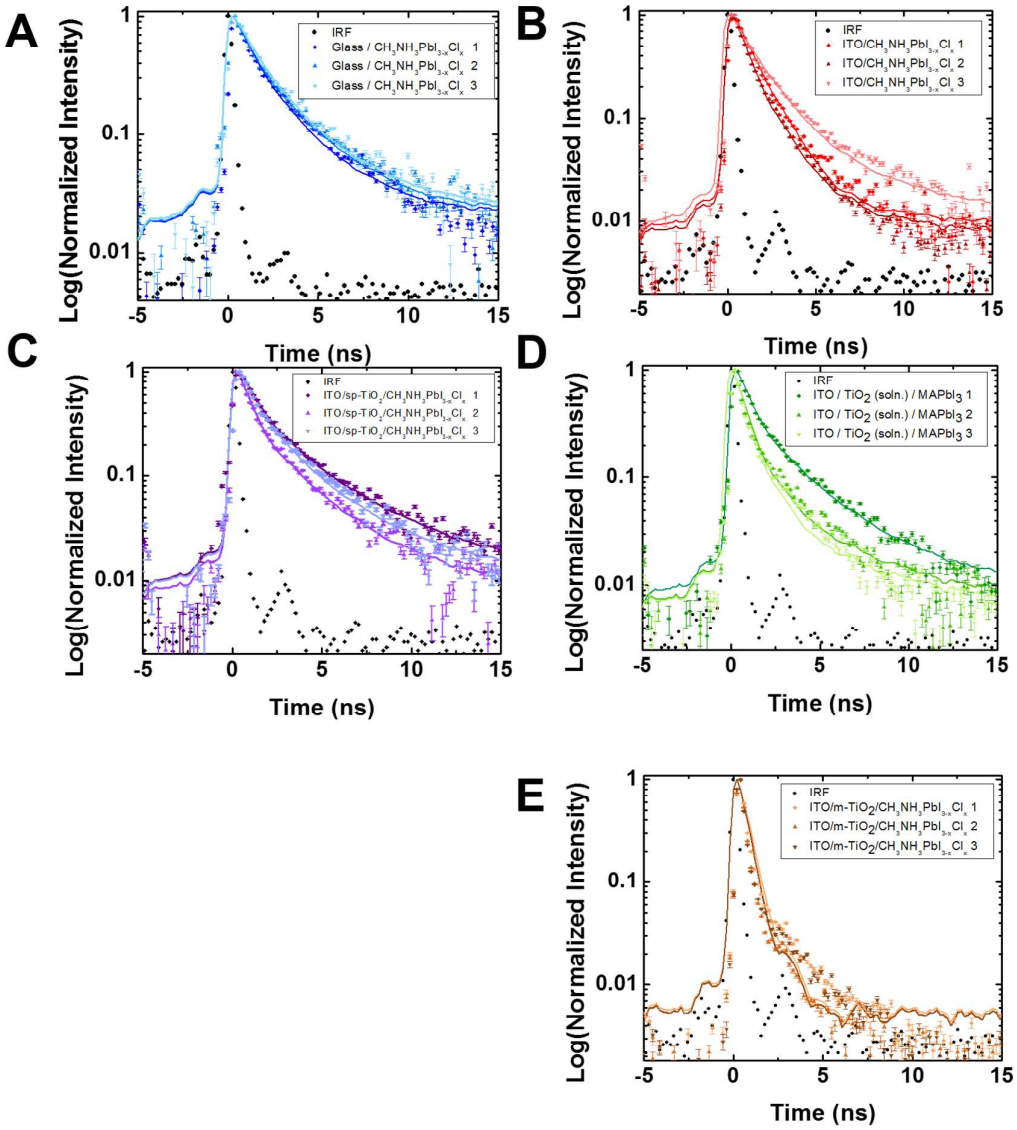

Figure S6. Normalized TRPL profiles and fitting curves for thin films comprising **A)** glass/$CH_3NH_3PbI_{3-x}Cl_x$, **B)** ITO/$CH_3NH_3PbI_{3-x}Cl_x$, **C)** ITO/sp-TiO_2/$CH_3NH_3PbI_{3-x}Cl_x$, **D)** ITO/b-TiO_2/$CH_3NH_3PbI_{3-x}Cl_x$, and **E)** ITO/m-TiO_x/$CH_3NH_3PbI_{3-x}Cl_x$ films.

Table S2. Average decays and relative amplitude for all $CH_3NH_3PbI_{3-x}Cl_x$ samples deposited on b-TiO_2, m-TiO_x, and sp-TiO_2, respectively. TRPL decays and amplitudes are also presented for all $CH_3NH_3PbI_{3-x}Cl_x$ samples deposited on bare glass and bare ITO.

Sample	τ_1 (ns)	Relative Amplitude	τ_2 (ns)
Glass/$CH_3NH_3PbI_{3-x}Cl_x$ (1)	0.99 ± 0.02	0.26 ± 0.02	2.88 ± 0.06
Glass/$CH_3NH_3PbI_{3-x}Cl_x$ (2)	0.94 ± 0.02	0.31 ± 0.02	2.94 ± 0.07
Glass/$CH_3NH_3PbI_{3-x}Cl_x$ (3)	1.17 ± 0.03	0.25 ± 0.03	3.34 ± 0.01
ITO/$CH_3NH_3PbI_{3-x}Cl_x$ (1)	1.115 ± 0.008	0.023 ± 0.006	3.7 ± 0.5
ITO/$CH_3NH_3PbI_{3-x}Cl_x$ (2)	0.82 ± 0.01	0.10 ± 0.01	2.3 ± 0.1
ITO/$CH_3NH_3PbI_{3-x}Cl_x$ (3)	1.29 ± 0.01	0.10 ± 0.01	4.0 ± 0.2
ITO/sp-TiO_2/$CH_3NH_3PbI_{3-x}Cl_x$ (1)	1.01 ± 0.01	0.26 ± 0.01	3.74 ± 0.05
ITO/sp-TiO_2/$CH_3NH_3PbI_{3-x}Cl_x$ (2)	0.68 ± 0.01	0.212 ± 0.007	2.88 ± 0.04
ITO/sp-TiO_2/$CH_3NH_3PbI_{3-x}Cl_x$ (3)	1.01 ± 0.01	0.23 ± 0.01	3.35 ± 0.06
ITO/b-TiO_2/$CH_3NH_3PbI_{3-x}Cl_x$ (1)	0.76 ± 0.01	0.24 ± 0.01	3.06 ± 0.06
ITO/b-TiO_2/$CH_3NH_3PbI_{3-x}Cl_x$ (2)	0.70 ± 0.01	0.071 ± 0.004	3.5 ± 0.1
ITO/b-TiO_2/$CH_3NH_3PbI_{3-x}Cl_x$ (3)	0.689 ± 0.004	0.050 ± 0.003	3.4 ± 0.1
ITO/m-TiO_2/$CH_3NH_3PbI_{3-x}Cl_x$ (1)	0.518 ± 0.001		
ITO/m-TiO_2/$CH_3NH_3PbI_{3-x}Cl_x$ (2)	0.468 ± 0.001		
ITO/m-TiO_2/$CH_3NH_3PbI_{3-x}Cl_x$ (3)	0.460 ± 0.001		